Wire Pad Chambers and Cathode Pad Chambers for the LHCb Muon System

CERN, PNPI, UFRJ

Contents

Chapter 1

Introduction

The task for the muon chambers in LHCb is to detect muons within a time window of 25ns with very high efficiency ($\geq$99%) with position resolution in X and Y ranging from 0.5 cm to 30 cm. We expect particle rates of up to 560 kHz/cm^2, so in addition the chambers have to cope with high rates and large charge deposits over 10 years of operation.

Wire Pad Chambers (WPCs) and Cathode Pad Chambers (CPCs) are able to satisfy all these requirements in all the regions of the detector. Table 1 show the rates and accumulated charge for the entire detector.

Except for Region1 and Region2 in M1 the total accumulated charge in 10 years of operation is less that 1 Coulomb/cm which was proven to be a safe range with respect to aging effects. The only detector limitation of WPCs and CPCs would be gas gain drop due to space charge effects in the detector gas which are however negligible up to rates of 1MHz/cm^2.

Two advantages of WPCs and CPCs we consider to be most important:

- **The technology can be used in almost the entire detector guaranteeing maximum uniformity.**
- **WPCs and CPCs are ordinary Multi Wire Proportional Chambers which are very robust and whose performance is very well understood and can be well simulated.**

Table 1.1: Rates and accumulated charge in the Detector for WPCs and CPCs. The charge is calculated assuming a gas gain of 1.6×10^5.

	Station	M1	M2	M3	M4	M5
R1	Rate/cm^2/interaction	7×10^{-3}	2.5×10^{-4}	2×10^{-4}	1.2×10^{-4}	1.2×10^{-4}
	Rate @ 5×10^{32} (kHz/cm^2)	280	10	8	4.8	4.8
	Rate/cm^2 + safety (kHz/cm^2)	560	50	400	24	24
	C/cm/10years @ 2.5×10^{32}	4.2	0.75	0.6	0.36	0.36
	Rate/channel wire pad (kHz)	–	780	730	500	580
	Rate/channel cathode Pad (kHz)	1400	590	550	500	580
R2	Rate/cm^2/interaction	4×10^{-3}	1.2×10^{-4}	2×10^{-5}	$1. \times 10^{-5}$	8×10^{-6}
	Rate @ 5×10^{32} (kHz/cm^2)	160	4.8	0.8	0.4	0.3
	Rate + safety (kHz/cm^2)	320	24	4	2	1.6
	C/cm/10years @ 2.5×10^{32}	2.4	0.36	0.06	0.03	0.024
	Rate/channel wire pad (kHz)	–	750	150	170	150
	Rate/channel cathode pad (kHz)	1600	560	220	130	120
R3	Rate/cm^2/interaction	1×10^{-3}	4×10^{-5}	4×10^{-6}	3×10^{-6}	3×10^{-6}
	Rate @ 5×10^{32} (kHz/cm^2)	40	1.6	0.16	0.12	0.12
	Rate/ + safety (kHz/cm^2)	80	8	0.8	0.6	0.6
	C/cm/10years @ 2.5×10^{32}	0.6	0.12	0.012	0.009	0.009
	Rate/channel cathode pad	1600	250	30	50	60
R4	Rate/cm^2/interaction	3×10^{-4}	5×10^{-6}	1×10^{-6}	7.5×10^{-7}	3×10^{-6}
	Rate @ 5×10^{32} (kHz/cm^2)	10	0.2	0.04	0.03	0.12
	Rate/ + safety (kHz/cm^2)	20	1	0.2	0.15	0.6
	C/cm/10years @ 2.5×10^{32}	0.18	0.015	0.003	0.002	0.009
	Rate/channel wire pad	1600	130	30	115	60

Chapter 2

Muon System Layout

The muon chamber layout is based on the concept of projectivity between the five muon stations. It is fully conform to the so called "logical layout" described elsewhere [1] and is built with the smallest possible number of different chamber types, corresponding to the 4 regions. In particular for regions 1 and 2 it represents an optimal solution from point of view of matching between granularity and number of FE-electronics channels required.

A schematic view of a quadrant of stations 1, 2 and 5 is given in Figures 2.1-2.3. They indicate as well the chamber dimensions for the various regions and stations.

2.1 Station 1

Due to the high occupancy in Station 1 the use of logical strips is not possible in any of the four regions. Furthermore, the logical pads to be used in the trigger have to be split further in regions 2-4 into smaller physical pads in order to stay with the total rate at around 1.5 MHz.

We envisage cathode pad readout in regions 1 to 3 and anode wire (pad) readout in region 4. The cathode pads in region 3 are easily accessible from the chamber sides as the chambers are only 20cm wide.

Since regions 1 and 2 are subjected to the highest rates within the muon system and the accumulated charge is well above 1C/cm over 10 LHC years (Table 1), cathode pad chambers as discussed in this note are not proposed for this area. Micro gap chambers [2] operated with the same gas mixture might be a possible candidate for this area.

2.2 Stations 2 to 5

Stations 2 and 3 have a similar layout and impose the strongest requirements from granularity point of view: 6.25 mm in x in region 1. However, since the occupancy is significantly smaller than in station 1, logical strips can be used.

The building blocks for regions 1 and 2 of these stations are small chambers, where the required x-granularity is given by anode wire pads and the y-granularity by cathode pads within the same chamber. Four of these building blocks are combined in a module for region 2, as depicted in Figure 2.4. For region 1 the building blocks have the same height but even less width (cf. Figure 2.5), in order to allow a modular structure of the whole system with acceptable channel occupancy. The two double layers in regions 1 and 2 are put together in such a way that the distance between the layers along the z-axis is only 2.5 cm. This reduces the hit multiplicity in the two layers due to particles traversing the system with some angle to a minimum and helps to keep the total thickness per station low. Space of about 3.5 cm for the FE-board with the amplifier-shaper-discriminator chips is foreseen on the sides of each building block in these regions.

Region 3 is made of chambers which have only cathode pad readout, similar to station 1. Several (physical) pads in the horizontal and vertical plane respectively are grouped together to form logical strips. This has the great advantage that no deterioration to the required time resolution is introduced by signal propagation in strips. Since the surface of a physical channel is anyway limited by the maximum capacitance, the number of additional (physical) channels is rather small (10-15%).

Region 4 is made of chambers with anode wire readout only, as in region 4 of station 1. Similar to region 3, physical pads are combined to logical strips in the horizontal and vertical planes.

Stations 4 and 5 have again a very similar layout. The readout of the chambers in the various regions follows the one for stations 2 and 3. However, the requirements in x-granularity are much less stringent.

2.3 General Aspects

The overlap of the chambers within a station has been studied in detail and is sketched in Figure 2.6. It demands minimal amount of space for a double layer of double gap chambers: 4 times the size of a double gap chamber (estimated to 60 mm) plus 50 mm for a central support structure, hanging from the top. We believe that 300 mm space per station is sufficient for single or double layer of double gap chambers.

The proposed layout leads to 160 chambers per layer. The 16 chambers of regions 1 and 2 of stations 2-5 are made of 4, 6 or 10 building blocks of small chambers, which are combined to modules as discussed above.

A muon system with two double gap layers in each station would lead to a total of 1600 chambers and a sum of 140000 physical channels (front-end channels), which are then combined to about 25000 logical channels. The cost estimate given in section 7.2 is based on this configuration.

Alternatively, one could think of a layout where station 4 is dropped and three layers of double gap chambers are used instead in stations 3 and 5, in order to define on one hand a good seed for the muon trigger processor (station 3) and to reject on the other uncorrelated background (stations 3 and 5).

Both configurations provide a very redundant and highly efficient muon system, which is of great importance in order to achieve the physics goal of LHCb.

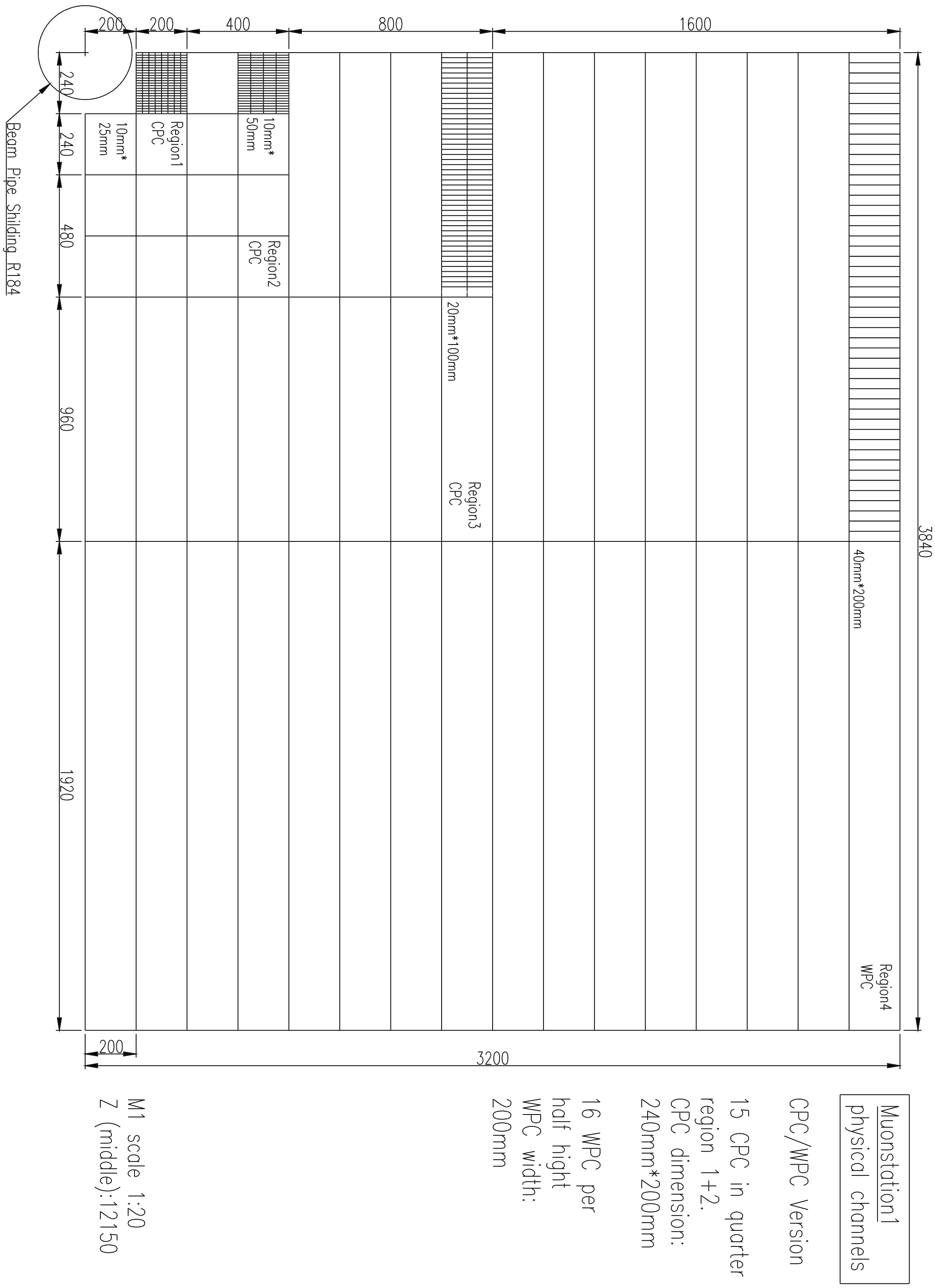

Figure 2.1 *: Layout of Station 1.*

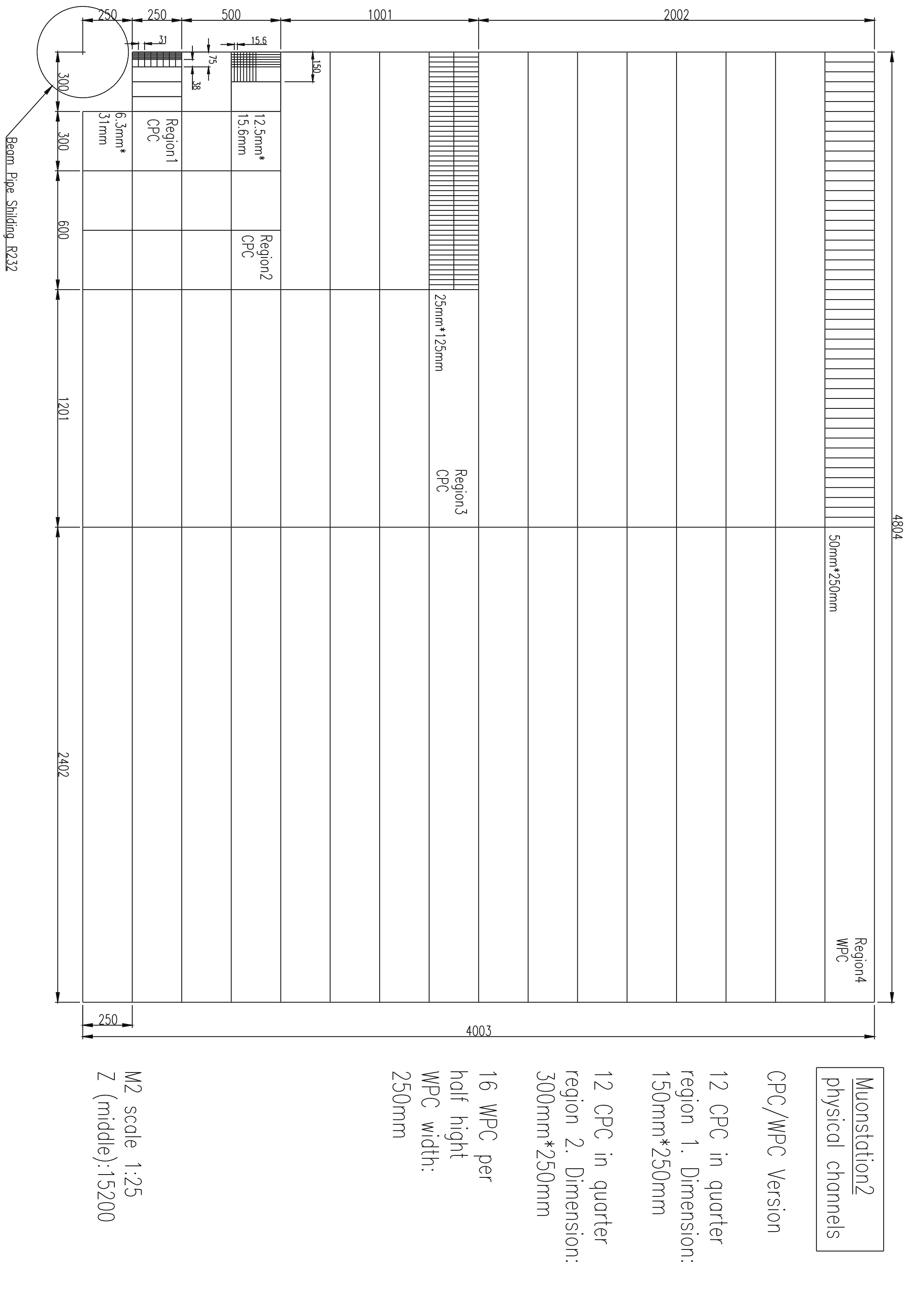

Figure 2.2 *: Layout of Station 2.*

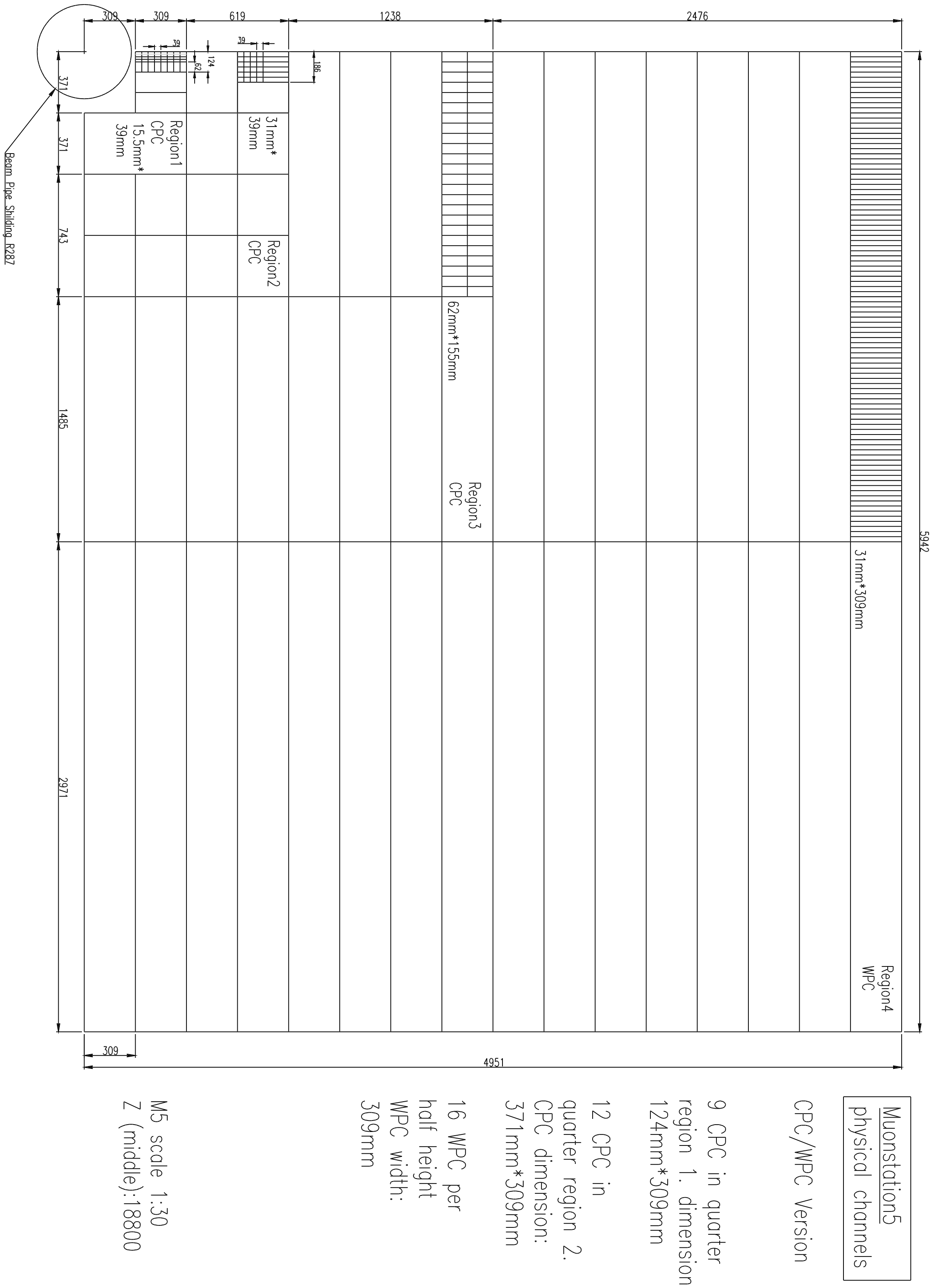

Figure 2.3 *: Layout of Station 5.*

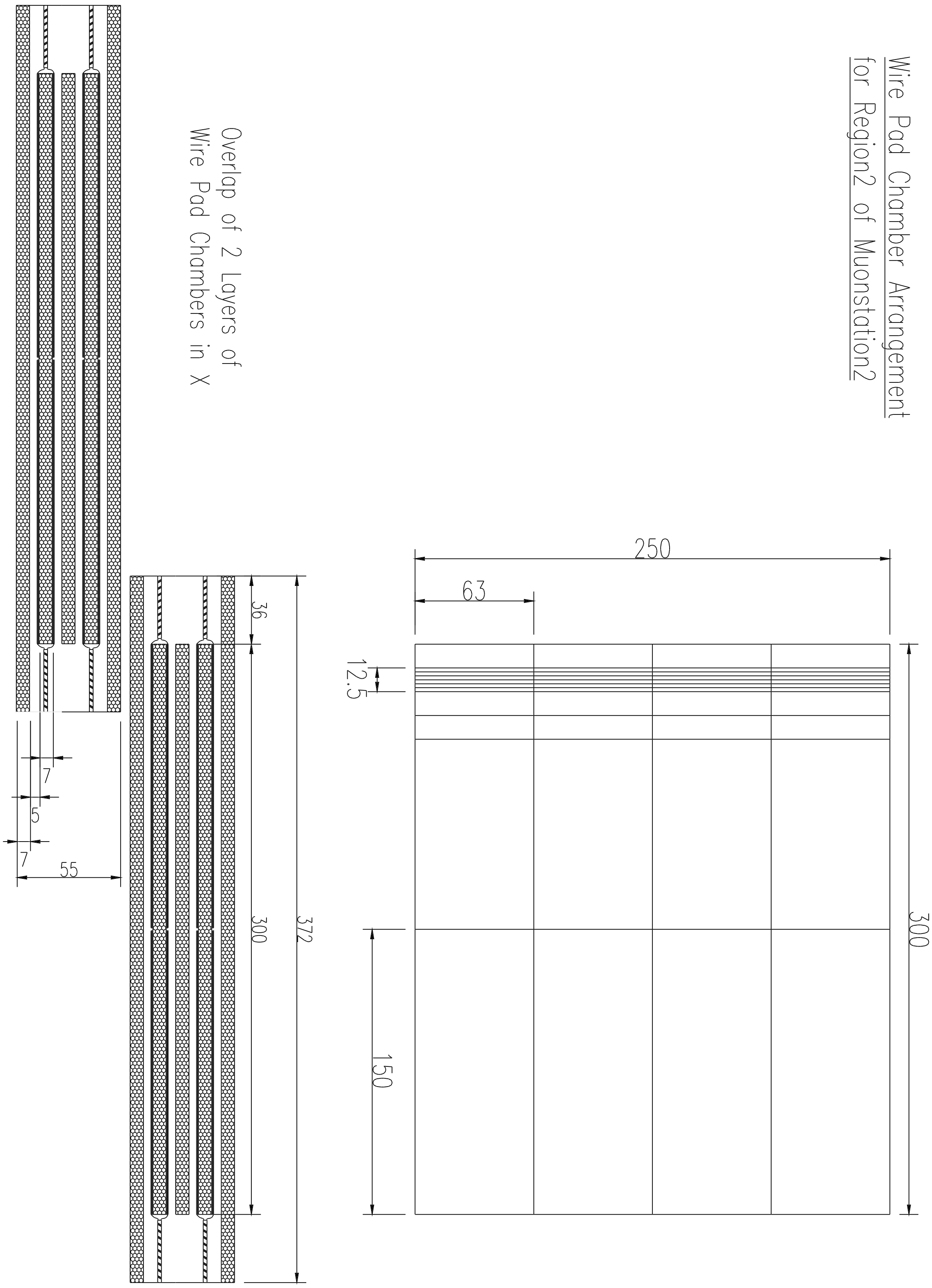

Figure 2.4 : *Building blocks for Region1 and Region2.*

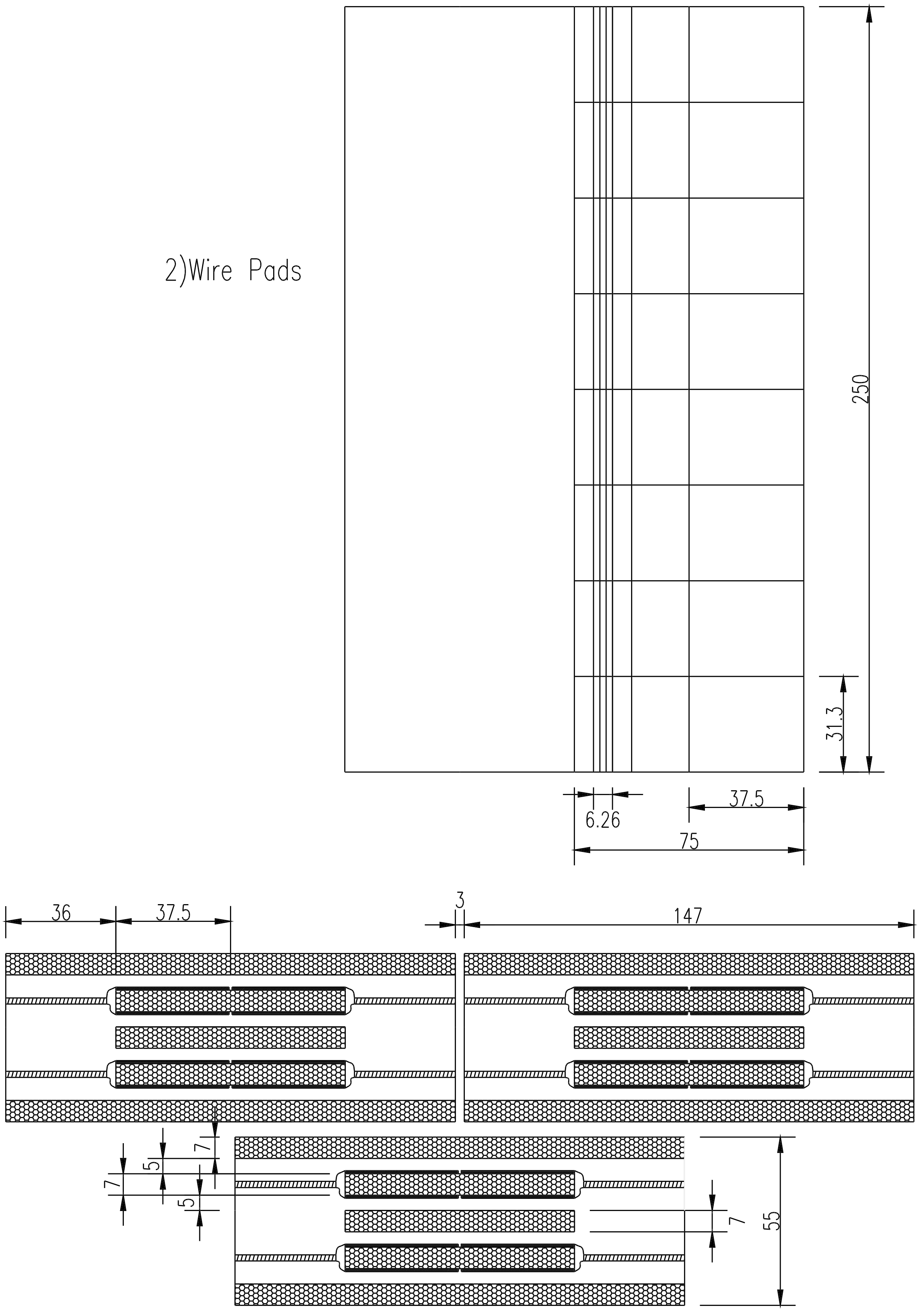

Figure 2.5 : *Detail of Region1 building blocks.*

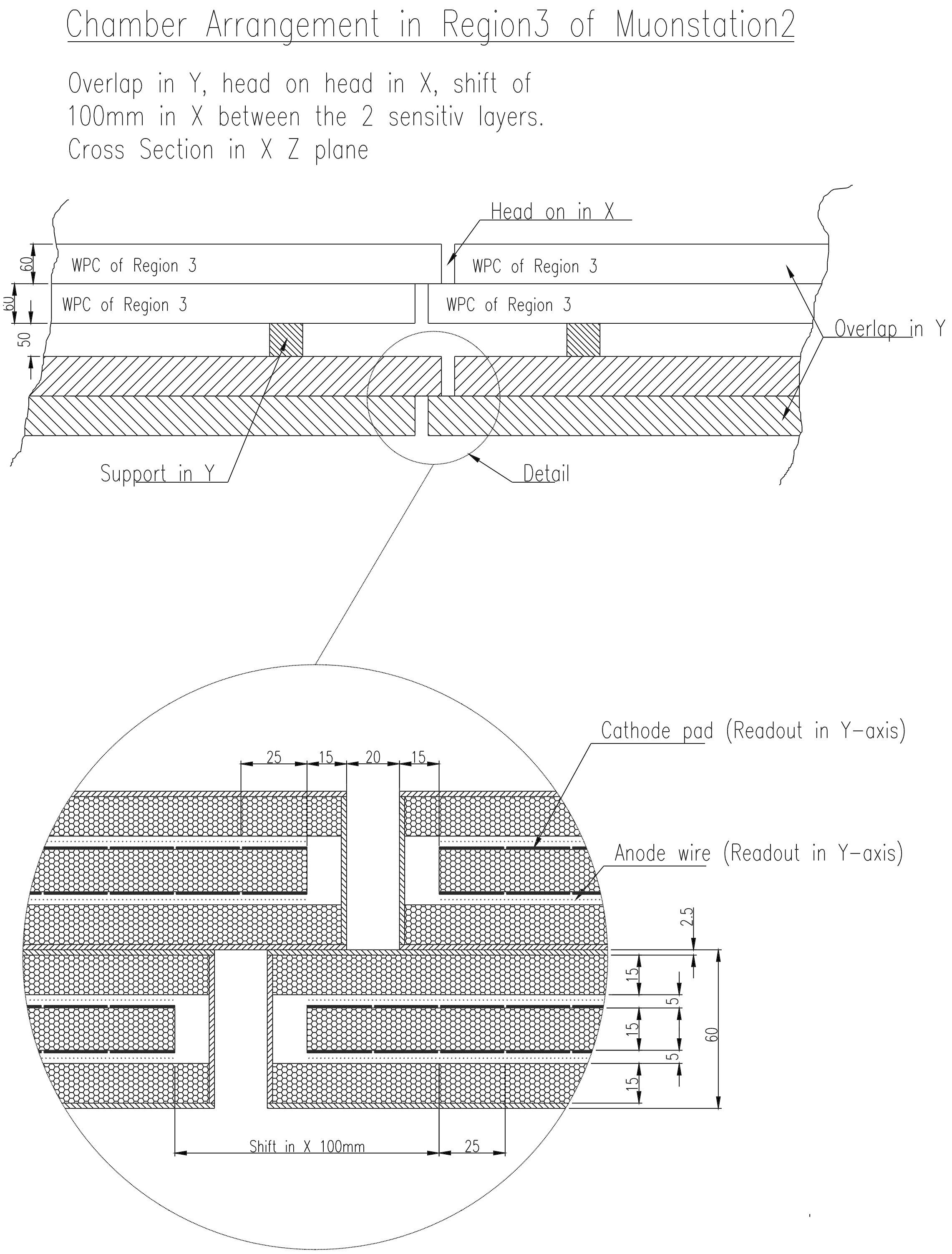

Figure 2.6 : *Detail of chamber overlap.*

Chapter 3

Geometry and Principle

The chamber geometry is shown in Fig. 3.1. One chamber consists of two gaps each having wires strung at a pitch of 1.5 mm. Some important parameters are listed in Table 3. A particle traversing these two gaps will ionize the gas leaving in total on average 100 primary electrons electrons (Fig. 3.2).

The electric field in the chamber is given by

$$r_c = \frac{s}{2\pi} e^{\frac{\pi h}{s}} \qquad E_a = \frac{V_a}{r_a \log(\frac{r_c}{r_a})} \qquad E_c = \frac{V_a \pi}{s \log(\frac{r_c}{r_a})} \tag{3.1}$$

where E_a is the field on the anode wire surface and E_c is the field on the cathode surface. For a voltage of 3000 V we find a cathode field of about 7900 V/cm, so for the discussion we can assume an average field in the drift region of about 8 kV/cm. Figure 3.3 shows the drift velocity for different gases as simulated by MAGBOLTZ.

The chambers operate at a gas gain around 10^5 which requires 3000 V for the Ar/CO_2/CF_4

cathode to cathode distance (2h)	5 mm
wire diameter ($2r_a$)	30 μm
wire pitch (s)	1.5 mm
equivalent cathode radius (r_c)	45 mm
gas	Ar/CO_2/CF_4 40/45/15
gain and voltage	10^5 @ 3000 V
breakdown limit	3300 V
gas	Ar/CO_2/$C_2H_2F_4$ 40/45/15
gain and voltage	10^5 @ 3100 V
breakdown limit	3700 V

Table 3.1: Some detector parameters.

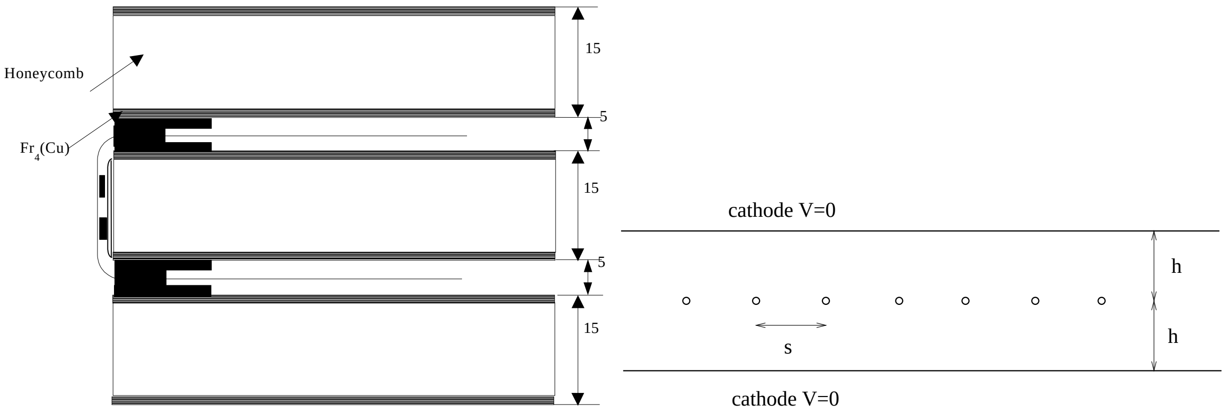

Figure 3.1 *: Cross section of a WPC or CPC chamber. The left figure shows the whole chamber, the right figure shows a single gap.*

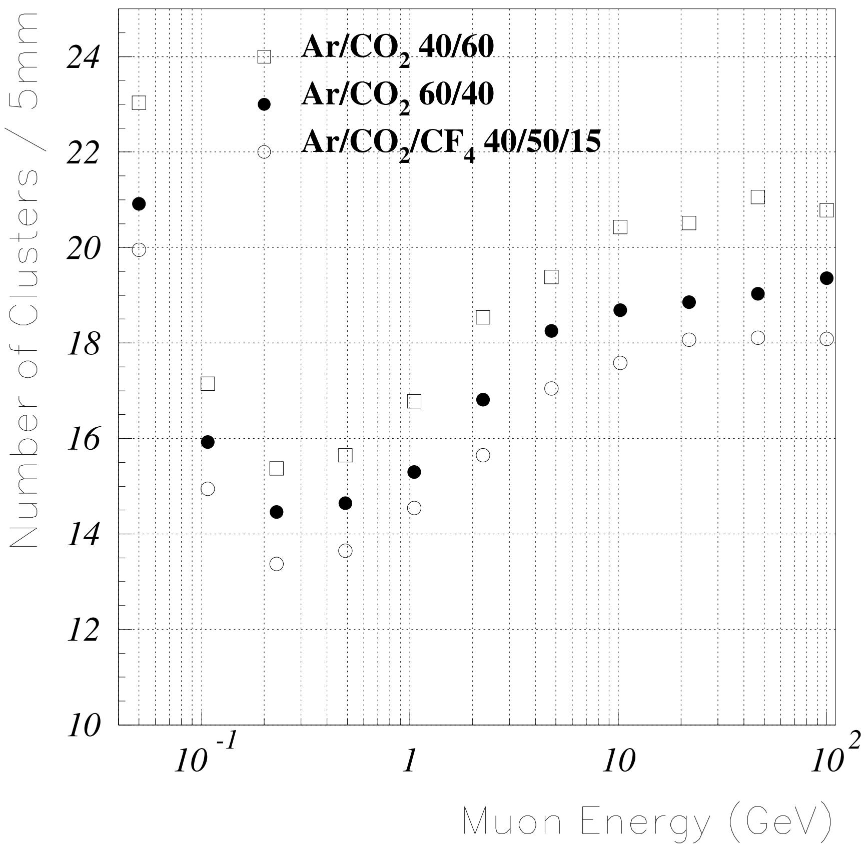

Figure 3.2 *: Number of clusters in a single gap as simulated with HEED. For a 10 GeV Muon we find about 20 clusters in a single gap, so with an average of 2.5 electrons/cluster we expect a primary ionization of 100 electrons.*

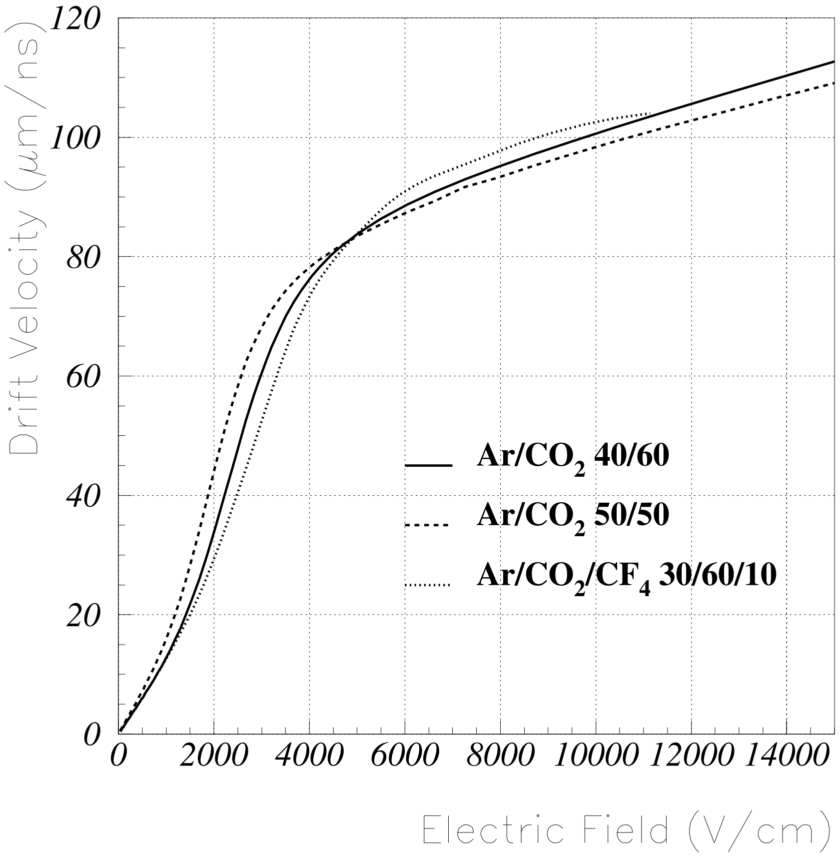

Figure 3.3 *: Drift velocity as a function of the electric field for different gases as simulated by MAGBOLTZ. The average electric field in the WPCs and CPCs is around 8 kV.*

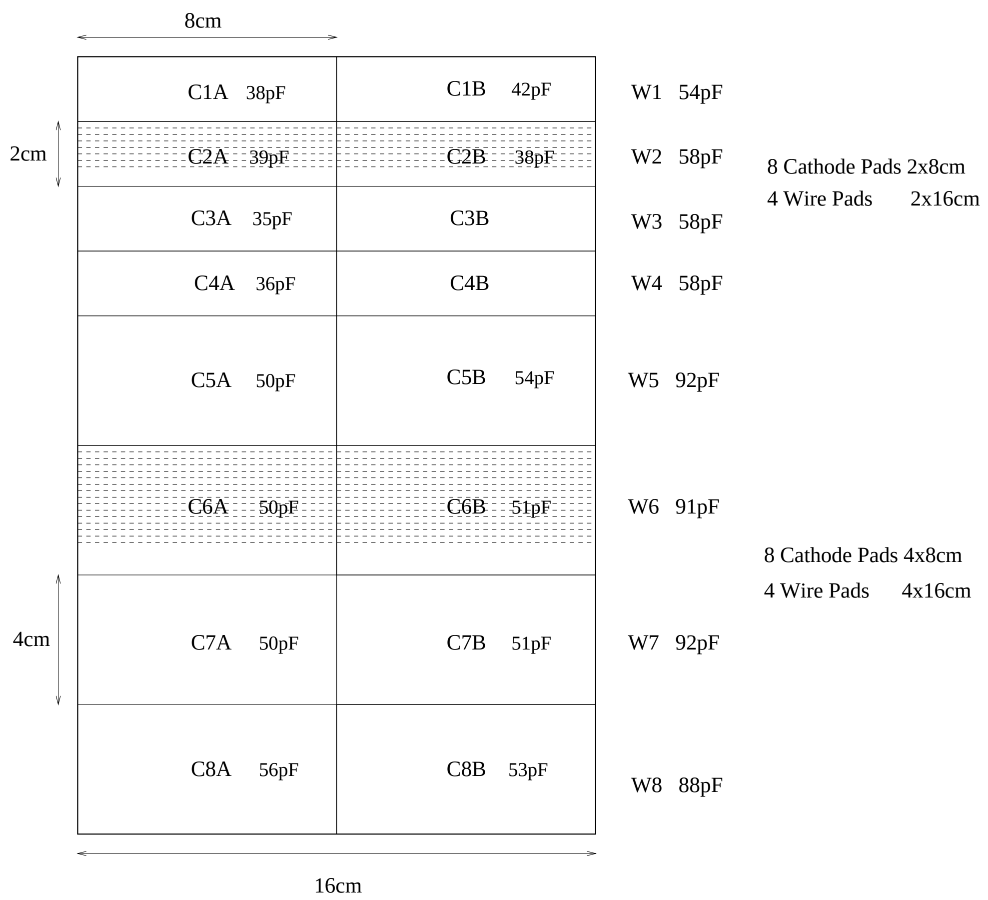

Figure 3.4 *: Schematic of a chamber prototype. The capacitance of the pads and the wires is the main source of noise.*

40/45/15 mixture and about 100 V more for the $Ar/CO_2/C_2H_2F_4$ mixture. The movement of the ions produced in the avalanche induces a negative current signal on the wire where the avalanche happened and a positive current signal on the neighbouring wires and the cathodes. Since the sum of all induced signals on all electrodes is zero, the signal induced on one cathode is exactly half of the wire signal.

By connecting several wires one gets a so called Wire Pad, by segmenting the cathode one arrives at a Cathode Pad. Figure 3.4 shows the segmentation of a prototype chamber that was used in the test beam.

The full width of half maximum of the charge distribution induced on the cathode pads is of the order of the anode - cathode spacing which is 2.5 mm in our case. A particle passing the chamber exactly between two pads will induce half the signal on both pads. If the particle crosses the chamber 2.5 mm from the edge of a pad, 90% of the charge is induced on one pad and only 10% is induced on the other pad. Since most of the cathode pads are several cm large, the 'cross talk' due to this effect is small.

Chapter 4

Electronics

In order to achieve good timing resolution at reasonably low gas gain, the front-end electronics is required to have short peaking time (around 10 ns) and low noise for detector capacitances of up to 200 pF. The high rates in some of the detector regions require in addition optimized tail cancellation and baseline restoration circuits as well as radiation hard technologies. Since the rates and occupancies vary strongly over the whole detector we might use different front-end chips in different detector regions. A few important system parameters for the current layout are listed in Table 4.1.

4.1 Signal Characteristics, Peaking Time

The movement of the avalanche ions induces a current of the form

$$i(t) = -\frac{q}{V} v(t) E(r(t)) = \frac{q}{2\log\frac{r_c}{r_a}} \frac{1}{t+t_0} \qquad t_0 = \frac{r_a^2 \log\frac{r_c}{r_a}}{2V_a \mu} \tag{4.1}$$

where t_0 has values between 1.5-2 ns for our geometry. The total charge induced after a time T is then

$$Q(t) = \frac{q}{2\log\frac{r_c}{r_a}} \log(1+\frac{t}{t_0}) \tag{4.2}$$

Fig. 4.1 shows the induced charge versus time for a single primary electron in the chamber and a gas gain of 10^5. This figure together with the fact that we expect on average 100

Max. Wire Pad Capacitance	200 pF
Max. Cathode Pad Capacitance	100 pF
Max. Rate per channel	1.6 MHz
Max. Dose	$\leq$ 1 MRad

Table 4.1: Some parameters determining the electronics environment. In a large part of the system the rates and doses are orders of magnitude smaller.

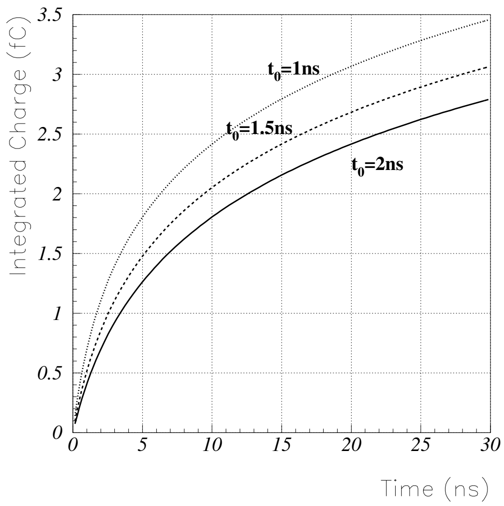

Figure 4.1 : *Integrated charge for a single primary electron and a gas gain of* 10^5.

primary electrons in the chamber sets the scale for the required front-end sensitivity.

4.2 Noise Characteristics

In addition to diffusion and the spatial distribution of the primary ionization electrons the resolution is affected by time slewing due to pulse height fluctuations (Fig. 4.2). This contribution is minimal for low threshold and fast signal rise time. The lowest possible threshold however is set by the noise which also depends on the front-end peaking time. The equivalent noise charge due to serial and parallel noise is given by

$$ENC^2 = \frac{1}{2} e_n^2 C^2 \int_{-\infty}^{\infty} f'(t)^2 dt + \frac{1}{2} i_n^2 \int_{-\infty}^{\infty} f(t)^2 dt \tag{4.3}$$

where $f(t)$ is the normalized front-end delta-response, C is the detector + input capacitance. The parameters e_n and i_n are the serial and parallel noise densities which depend on the front-end design and technology. Typical values are $e_n \approx 1 - 2\, nV/\sqrt{Hz}$ and $i_n \approx 2 - 3\, pA/\sqrt{Hz}$. Approximating the signal leading edge by a straight line and setting the threshold to the lowest possible value ($5\,\sigma$ of the noise) we find the time slewing contribution to be

$$\sigma_t \propto \frac{t_p e_n C \sqrt{a t_p \frac{i_n^2}{e_n^2 C^2} + \frac{b}{t_p}}}{G \times \log(1 + \frac{t_p}{t_0})} \tag{4.4}$$

where a and b are dimensionless constants characterizing the shape of the delta response and G is the gas gain. We see that the time slewing effect is proportional to the detector capacitance and inversely proportional to the gas gain. The function has a minimum at $t_p \leq 3.92\, t_0$, so the optimum peaking time for the WPCs and CPCs is $\leq 8\, ns$. Since very

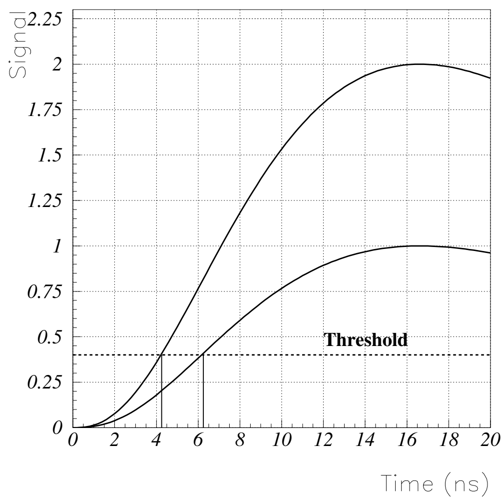

Figure 4.2 : *Pulse height fluctuations will result in threshold crossing time fluctuations (time slewing).*

high bandwidth amplifiers are not desired in a large system we want a peaking time around $10\,ns$.

4.3 Front-end input resistance and capacitance

The capacitance determining the serial noise is the detector capacitance plus input capacitance. Therefore the input capacitance should be as low as possible. The detector capacitance C_{det} together with the front-end input resistance R_{in} define a time constant $\tau_{in} = R_{in}C_{det}$ which acts as an integration stage. Therefore the chamber signal effectively 'sees' a circuit which consists of an integrator together with the preamp circuit, i.e. R_{in} and C_{det} decrease the system peaking time. In order to limit this peaking time dependence on the detector capacitance the input resistance should be as small as possible.

4.4 Tail cancellation

In the LHCb muon system we expect rates per channel of up to 1.6 MHz. In order to minimize the inefficiency due to signal pile-up the signal pulse width has to be as short as possible. Fig. 4.3 shows the inefficiency due to pile-up for different rates and pulse width. Since the wire chamber signal has a very long tail we need a dedicated filter circuit to achieve this goal.

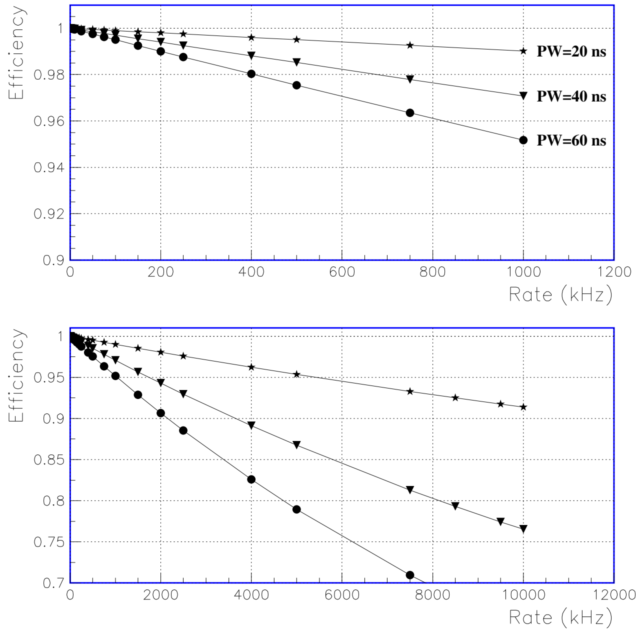

Figure 4.3 *: Efficiency for a time window of 25 ns and different rates and pulse widths for uncorrelated background.*

4.5 Baseline Restoration

In order to avoid baseline fluctuations due to high channel occupancies the front end should use either a bipolar shaping circuit or a dedicated baseline restoration circuit. Since bipolar shaping increases the dead-time by almost a factor 2, a unipolar shaping scheme together with a baseline restorer is favoured.

4.6 Candidate Electronics

Two types of electronics were used for WPC and CPC tests, one other candidate is currently under investigation and a dedicated chip development program is under way at CERN. Their characteristics are summarized in Table 4.2. The 'PNPI electronics' consists of a preamplifier and a separate main amplifier realized as discrete SMD components. This electronics is optimized for this type of WPC and CPC chambers and will therefore be used as our reference showing the optimum performance of the chamber. As it is built with discrete components it is considered not practical for our application.

model	PNPI	SONY	ASDQ
technology	discrete comp.	SONY Bipolar	MAXIM Bipolar
input resistance	25 Ω	80 Ω	260 Ω
peaking time @ C_{det}=0	4 ns	11 ns	8 ns
peaking time @ C_{det}=100 pF	7 ns	20 ns	
ENC @ 10 pF	1800 e-	1500 e-	2300 e-
sensitivity @ C_{det}=0	10 mV/fC	5.6 mV/fC	3 mV/fC
sensitivity @ C_{det}=100 pF	6 mV/fC	3.5 mV/fC	
Radiation Limit		$\geq$50 kRad	$\geq$ 5 MRad
Av. Pulsewidth @ 100 pF	60 ns	90 ns	25 ns
Baseline restoration	no	yes	yes
Max. rate tested		1 MHz	15 MHz
Channels/Chip		4	8
Power Consumption/channel		59 mW	40 mW
Cost per Channel		1.7 SFr	4 SFr

Table 4.2: Some electronics parameters.

The so called 'SONY chip' [3], was developed for the ATLAS TGC chambers and is a possible candidate for use in LHCb. This chip is however slower and, due to its high input resistance, the performance degrades quickly for large input capacitances. Moreover the chip is not sufficiently radiation hard for the innermost regions of the muon system. Therefore it is only suitable for the outer regions where the dose rate is low and the use of high gas gain doesn't lead to aging problems.

For the high rate regions we consider the ASDQ chip [4] which is a modified version of the ASDBLR chip [5] used for the ATLAS TRT. The ASDQ was developed for the central tracking chamber (COT) at CDF and has the additional feature of performing a charge measurement which is encoded in a pulse width. It is radiation hard, has a tail cancellation circuit and an active baseline restorer. Since the signal shape of the WPC and CPC chambers is very similar to the TRT and COT, the tail cancellation circuit is well adapted for our needs. The output pulse width is 25-30 ns if used in time-over-threshold mode and 45-50 ns if used in the charge encoding mode. Since the input impedance is very high (280 Ω) the chip is only suited for small capacitances.

A new chip development using a 0.25 μm CMOS technology which is expected to be radiation hard is currently under way at CERN. If successful, this chip would also be a candidate for the high rate environment.

Chapter 5

Performance

Several WPC and CPC prototypes were tested in the T7 and T11 beams at CERN. A CPC prototype with various pad sizes (from $1 \times 2\,\mathrm{cm}$ to $8 \times 16\,\mathrm{cm}$) was constructed and tested in autumn 1998, using the readout design presented in the Technical Proposal [7] and was shown to be reliable.

A first WPC prototype with wire pad readout only was tested in May 1999. Further WPC prototypes have been tested in November 1999. They contained cathode strips as well as cathode pads. Here we present results from the prototype shown in Fig. 3.4, with wire pads $4 \times 16\,\mathrm{cm}^2$ large and cathode pads $4 \times 8\,\mathrm{cm}^2$ large.

Figure 5.1 shows the efficiency as a function of the high voltage for the gas $Ar/CO_2/C_2H_2F_4$ 40/45/15 using the Sony chip. Cuts were applied in the charge and number of hits in the scintillators in order to select single particle events. For a time window of 25 ns the chamber is fully efficient at a voltage of 3.25 kV corresponding to a gas gain of 2×10^5. To get to 99 % efficiency in 20 ns, it is necessary to operate at higher gain, namely at 3.4 kV. The chamber was operated up to 3.7 kV before breakdown occured. Hence, in the outer detector regions, where the rates and therefore the total charge deposits are low, one has still a large operating plateau of 300 V which is very convenient. Figure 5.2 shows an example of the time distribution at the working point. The time resolution (RMS) is about 3.0-4 ns for the anodes and 3-4.5 ns for the cathodes in the operating range of 3.25 -3.5 kV. The measured shift of the mean arrival time is about 1.5-2 ns / 100V.

As discussed in the last section, the peaking time and the sensitivity of the Sony chip decreases rapidly for increased input capacitance. Therefore, in addition to the chamber geometry, the time resolution is largely influenced by the electronics. Using optimized electronics one can improve the performance to arrive at high efficiency even for lower gas gain. Fig. 5.3 shows a comparison between the efficiencies obtained with Sony chip and PNPI electronics for the standard gas mixture $Ar/CO_2/CF_4$ (40/45/15). Fig. 5.4

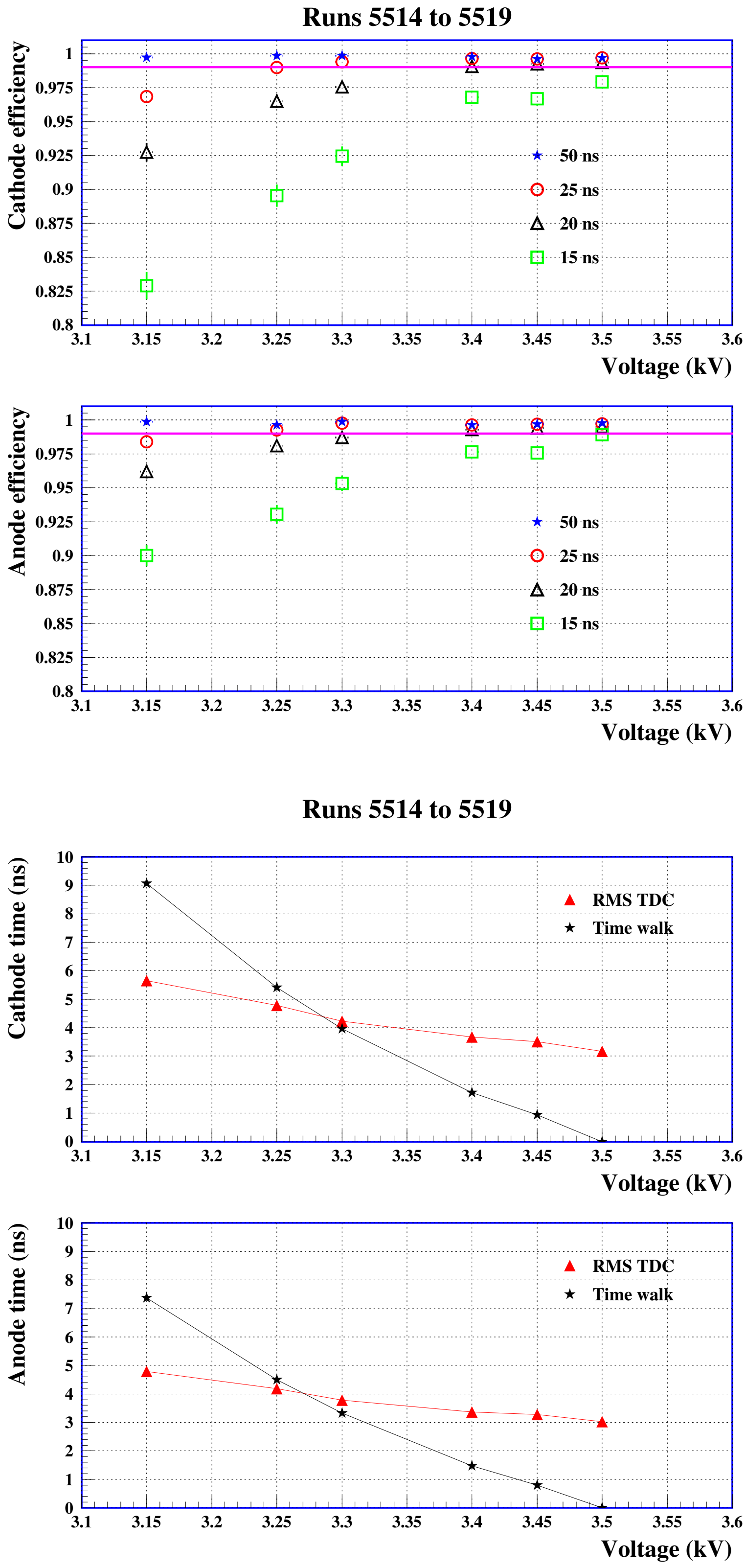

Figure 5.1 *: Efficiency versus voltage for different time windows for the gas* $Ar/CO_2/C_2H_2F_4$ *using the Sony chip. The cathode pads are* 4×8 *cm, the wire pads (anode) are* 4×16 *cm. The bottom figure shows the time rms and the mean arrival time shift versus voltage.*

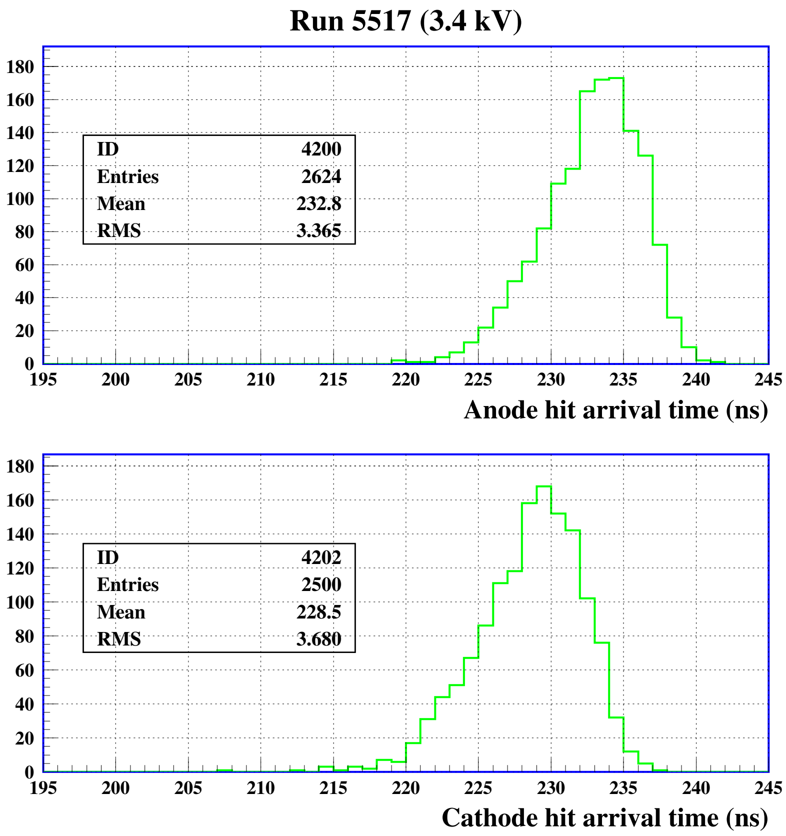

Figure 5.2 : *Time distribution at the working point for cathode and anode pads.*

Table 5.1: Percentage of events with hits in the neighbouring pads within 20 ns

Electronics	gas mixture	Gas Gain	Anode pads	Cathode pads
a) PNPI	$Ar/CO_2/CF_4$	2×10^5	4 %	3 %
b) SONY	$Ar/CO_2/CF_4$	2×10^5	5%	4%
c) SONY	$Ar/CO_2/C_2H_2F_4$	4×10^5	20 %	13 %

Table 5.2: Deterioration in the B→ μX efficiency.

	Region II	Region III	Region IV
b) SONY & $Ar/CO_2/CF_4$	xx%	xx%	
c) SONY & $Ar/CO_2/C_2H_2F_4$	xx %	xx %	

compares the time resolution for the PNPI and SONY electronics.

To study crosstalk, events were selected using the best possible choice of hodoscope channels, in order to have the particles crossing the center of the pad and still have enough statistics. Table 5 presents the percentage of events which have more than one hit within the 20 ns time window. Since the gas $Ar/CO_2/C_2H_2F_4$ allows operation of the chamber at higher gas gain, which is necessary for thew SONY chip, the increase of crosstalk at the corresponding voltage is explained. Optimizations can be done to decrease the capacitive coupling between the pads, reducing then the crosstalk and cluster size. For the time being, the impact of those results in the trigger performance was studied using the cluster size distributions for cases b) and c), showed in figure 5.5. Table 5 shows the deterioration in the efficiency of the trigger for B→ μX events, normalized to the same minimum bias retention obtained when no crosstalk is included.

In order to analyse the dependence of the efficiency on rate, including pile-up effects, events were selected with at least one hit in the scintillators facing the pad and no cut on the charge was applied. Events with hits on the hodoscope strips facing neighboring pads were rejected, in order to reduce crosstalk and other effects.

Figure 5.6 shows the efficiency as a function of the rate measured in the anode pads equiped with SONY electronics. The gas gain is 2×10^5. The efficiency in 20 ns is reduced by $\sim$2% when the rate increases to $\sim$720 KHz.

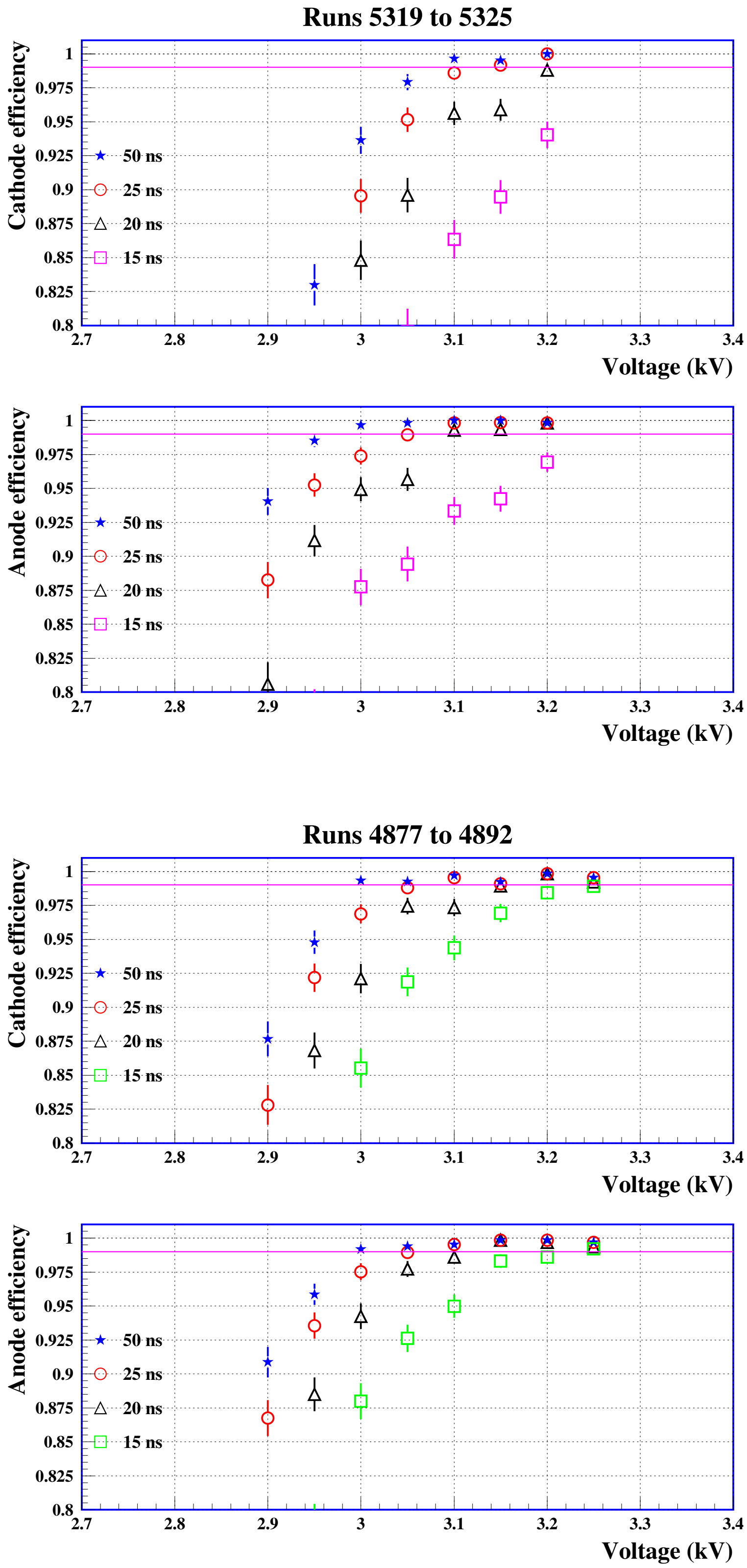

Figure 5.3 : *Efficiency versus voltage for the gas Ar/CO_2/CF_4 40/45/15. The top figure shows the performance using the Sony chip, the bottom figure shows the performance using the PNPI electronics. For this gas a gain of 2×10^5 requires 3.15 kV.*

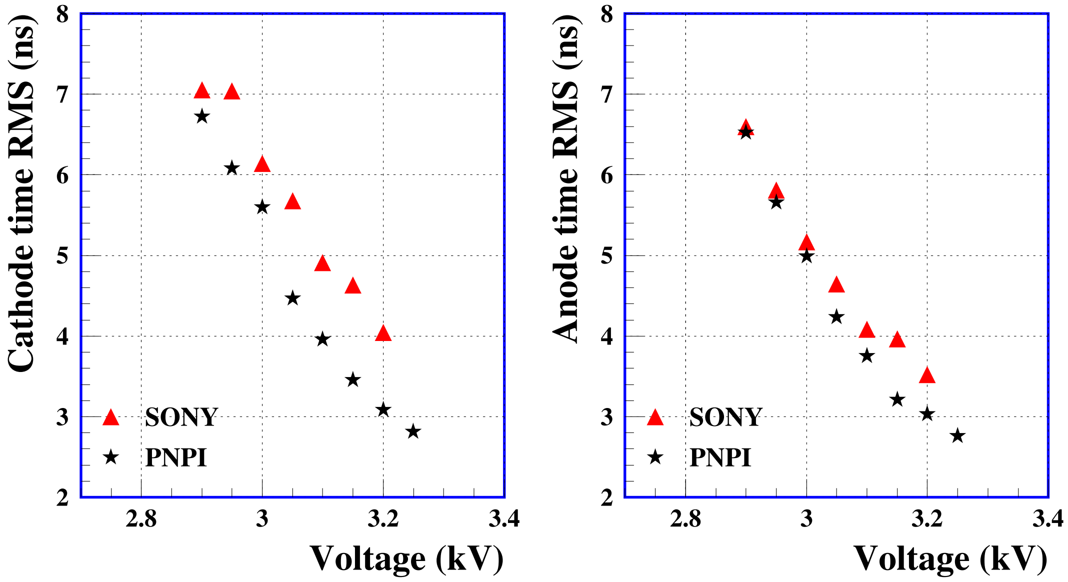

Figure 5.4 *: Time resolution for PNPI and SONY electronics.*

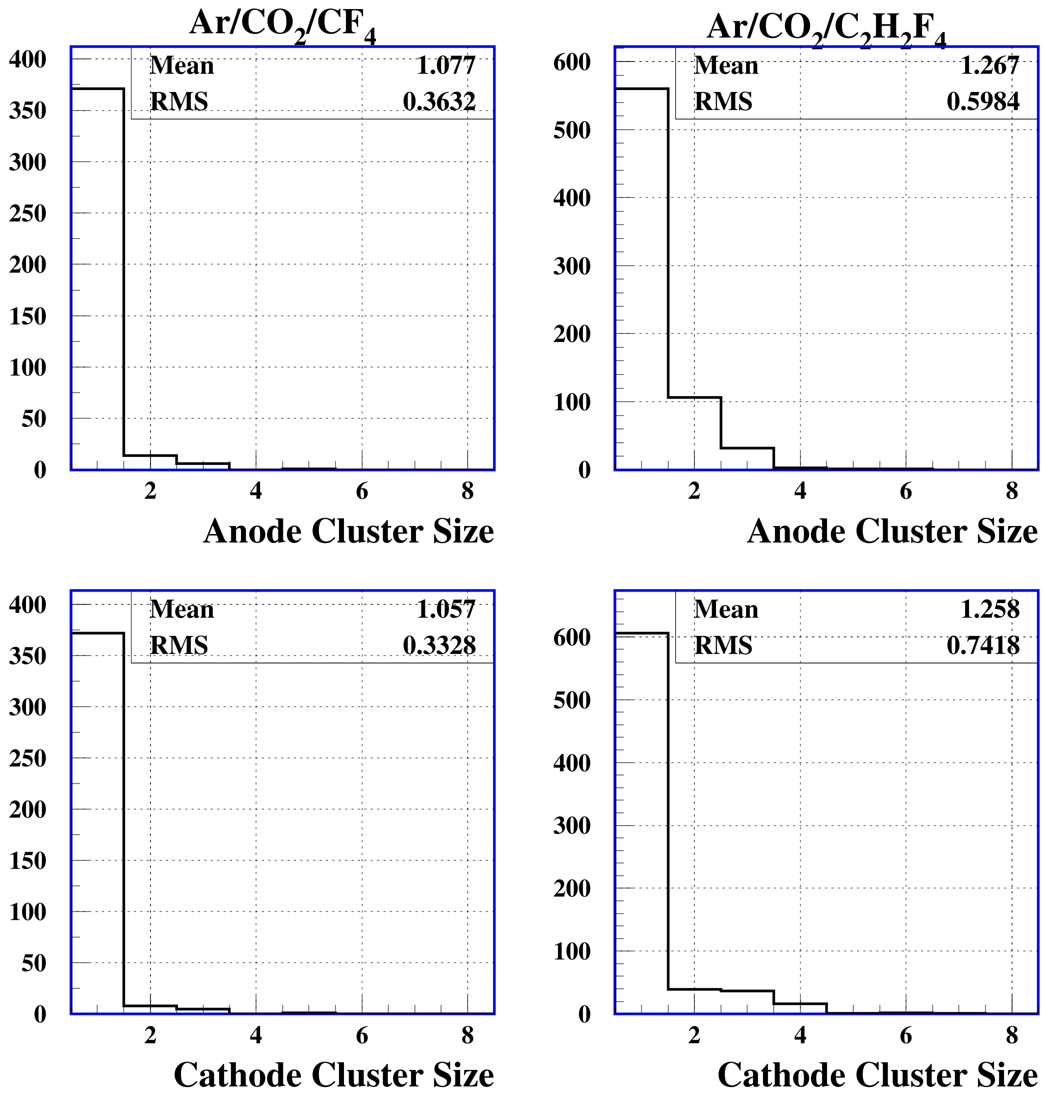

Figure 5.5 *: Cluster size distributions for anode (top) and cathode (bottom) for gas mixtures based on* $Ar/CO_2/CF_4$ *(left) and* $Ar/CO_2/C_2F_2H_4$ *(right) with the SONY electronics.*

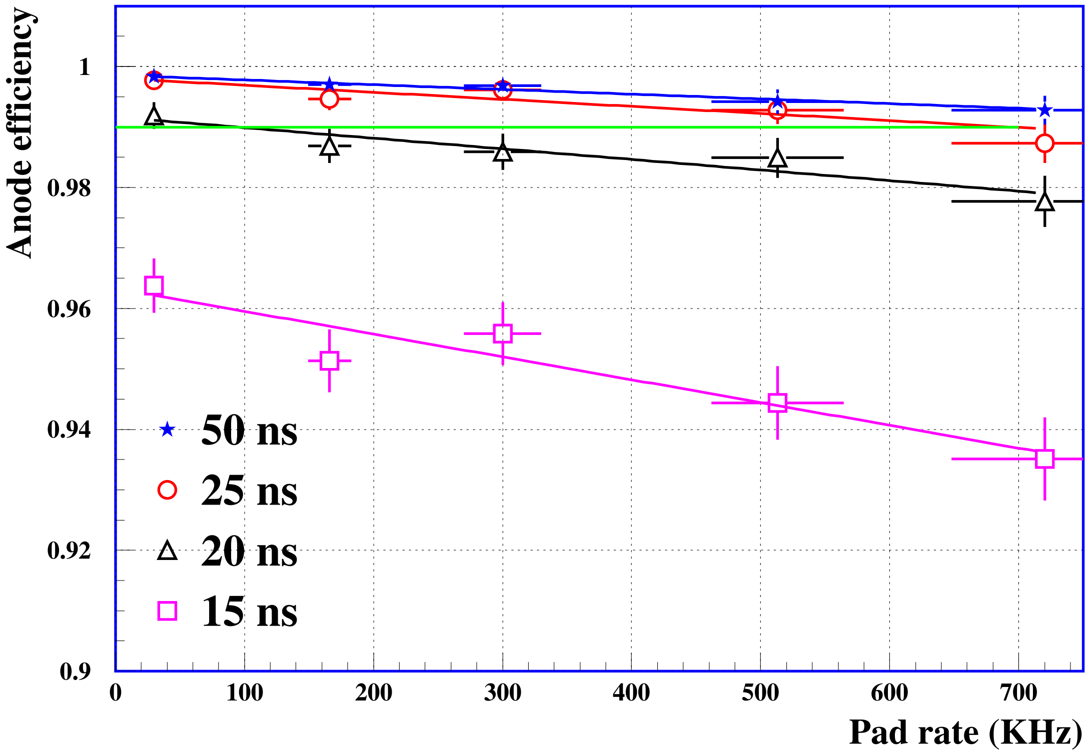

Figure 5.6 *: Efficiency versus rate for several time windows (SONY electronics).*

Chapter 6

Ageing

Detailed ageing studies of the wire chambers have been performed at PNPI in the framework of the CMS End Cap Muon System programme (CMS Note 1999/011). One should stress that the WPC/CPC chambers are made precisely from the same materials as the CMS chambers and use the same gas mixture. Therefore, the results obtained for the CMS chambers are directly applicable to the proposed WPC/CPC chambers. These tests showed that with the gas mixtures $Ar/CO_2/CF_4$ in the relative proportions 30/50/20 as well as 40/50/10 the deterioration of the chamber performance (gas gain and dark currents) was not observed up to the accumulated charges of 13 Coul/cm wire. Note however that the irradiation of the chambers was local with a Sr-90 beta source.

The global irradiation tests of the CMS chambers have been started last year at GIF facility at CERN. So far only a modest accumulated charge has been collected (0.2 Coul/cm wire). These tests will be continued in March/April 2000. We are planning to perform the local ageing tests at PNPI with the $Ar/CO_2/C_2H_2F_4$ gas mixtures using a WPC prototype. These tests will be started in Feb 2000. Also global ageing tests of the WPC filled with the $Ar/CO_2/C_2H_2F_4$ gas mixture are planned to be performed at GIF in March/April 2000 in parallel with the CMS tests.

Chapter 7

Realization

7.1 Construction

The WPC/CPC chambers are specially designed to make their construction as simple as possible. The wires are wound along the short side of the chamber that make it possible to use the small wire spacing (1.5 mm) needed for good time resolution without additional support structure. The WPC chambers use simple cathode planes without any pad/strip structure. There is no severe requirement to the flatness of the cathode plane to be produced in industry.

The FE electronics is arranged in a very simple way on the chamber body. The construction of such chambers can be easily organised in any physics laboratory. The WPC chambers will be used in region 4 of the LHCb Muon System covering about 75% of the total area. The CPC chambers designed for region 3 have a very simple cathode pad structure : 2 rows of $4 \times 10\,\mathrm{cm}^2$ pads with readout from both sides of the chamber. The construction of these chambers is not much different from the WPC construction. A similar type of construction will be used in region 2 and 1 of M2 - M5.

The most delicate task is the construction of the chambers for region 1 and 2 of M1. These chambers have a more complicated pad structure: four rows of $2 \times 5\,\mathrm{cm}^2$ pads in region 2 and eight rows of $1 \times 2.5\,\mathrm{cm}^2$ pads, both with the back-side read out system. An option using Micro Gap Chambers is considered at present but it needs still some R&D studies.

PNPI has many years experience in wire chamber construction. At present the institute is involved in the construction of the Cathode Strip Chambers for the CMS End Cap Muon System [8] which has close similarity with the LHCb chambers. PNPI can organise a special production line of the WPC/CPC chambers and would be able to assemble an essential part of these chambers. The production scheme assumes that there will be at least one more production line in some other laboratory and that the major parts for the chambers will be produced by collaborating groups with involvement of industry.

Chambers	Cu-panels	150-200 SFr/m^2
	Wires 0.15 SFr/m^2	200-300 SFr/m^2
	Spacers	100 SFr/m^2
	Alu Frames etc.	80 SFr/m^2
	for total 870 m^2	950 kSFr
	Assembly	40 manyears
Electronics	Fe board and chip	850 k
	short LVDS links	350 k
	intermediate boards	350 k
	Off detector electronics	500 k
	VME crates+controller	200 k
	total	2250 k
	tests and assembly	20 manyears
Service Systems	HV	450 k
	LV	70 k
	Gas system	200 k
	total	720 k
Various	supports	250 k
	tooling	200 k
	Iron Filter modif	500 k
	monitoring	50 k
	total	1000 k
Total Sum		4920 k
	with contingency of 10%	5410 k

Table 7.1: Cost overview.

7.2 Costing

Table 7.2 shows the cost estimates for the muon system. To estimate the manpower we considered one chamber per week per person. The contribtutions to the total cost which are technology specific are mainly the chambers, FE-chip and boards and HV-system and gas system, thus slightly less than 2450 kCHF. Some of the estimates for parts of the electronics chain need further substantiation. As the total budget for the muon system is about 6000 k, the final sum leaves about 500 k available for manpower.

Chapter 8

Conclusions

- WPCs and CPCs have shown to satisfy the requirements for almost the entire LHCb muon system.
- Except for Region 1 and Region 2 in M1, the accumulated charge in 10 years of operation is less that 1 C/cm.
- For Regions 3 and 4 in stations M3 to M5 the rates are low enough to allow a gas gain of up to 5×10^5, hence using the SONY chip will provide satisfactory operation.
- For M1 and the inner regions of M2-M5 the high rates require gas gain less than 2×10^5, so for safe operation a front end electronics chip must be found that matches the performance of the PNPI chip and also can stand a dose of up to 1 MRad.
- Detectors similar to CPC's but with different gain and geometry are under development for the hot spots in M1.

Bibliography

[1] P.Colrain et.al, LHCB-MUON-Note in preparation

[2] S. Getz et. al, Micro-Gap Chambers for the Inner Region of the LHCb Muon System, LHCb-Muon-Note

[3] O. Sasaki et. al., Amplifier-Shaper-Discriminator ICs, ATLAS internal muon note, Oct. 1999

[4] W.Bokhari et al., The ASDQ ASIC, CDF internal note, April 1998.

[5] ATLAS inner detector TDR. CERN/LHCC/97-17, M. newcomer et al., ASDBLR chip operational studies at CERN, ATLAS internal note 29.1. 1996.

[6] Wire Pad chambers for the LHCb muon system. LHCb internal note.

[7] LHCb Technical Proposal, CERN/LHCC 98-4, LHCC/P4, 20 February 1998

[8] CMS MUON TDR, CERN/LHCC 97-32, CMS TDR 3, 15 December 1997